A Multi-Wavelength Thulium-Doped Fiber Laser Using a Photonic Crystal Fiber-Based Sagnac Loop

Ting Li, Fengping Yan, Wenguo Han, Ting Feng, Ying Guo, Qi Qin, Zhuoya Bai, Dan Cheng, and Dandan Yang

***Abstract*—A multi-wavelength thulium-doped fiber laser incorporating a photonic crystal fiber (PCF) Sagnac loop was presented and experimentally demonstrated. In the laser cavity, the Sagnac loop mirror used a 0.5 m PCF as a comb filter. A nonlinear polarization rotation (NPR)-based 600 m single-mode fiber (SMF) was used to suppress the mode competition. By adjusting the polarization controllers (PCs), up to nine stable wavelength outputs near the 2 μm spectrum were obtained at room temperature with an optical signal-to-noise ratio (OSNR) of up to 30 dB. The channel spacing of this fiber laser is 4.88 nm, and the 10 dB bandwidth encompasses 1950.39 to 1989.43 nm.**

***Index Terms*—Multi-wavelength fiber laser, photonic crystal fiber, Sagnac loop mirror, NPR.**

I. Introduction

THULIUM-doped fiber lasers (TDFL) are of great interest due to their superior transmission and absorption properties. The operating band of TDFLs is 1.6 to 2.1 μm. This wavelength range is within the safe band of human eyes, and there are strong absorption peaks of various gas molecules, including H2O, CO2, and NH3 [1]–[3]. Therefore, TDFLs have incomparable advantages in many fields, notably gas molecular detection, laser radar, laser medical treatment, and modern optical communication systems [4]–[6].

In modern optical communication systems, fiber lasers that stably output multiple laser wavelengths allow wavelength division multiplexing (WDM) technology [7]–[9]. In 2016, W. He *et al.* proposed a Thulium-doped fiber laser based on a Sagnac ring and a Mach-Zehnder interferometer, which achieved a stable laser output from a single wavelength to a maximum of three wavelengths. The tuning range of the single-wavelength laser was 22.5 nm and the wavelength interval was 2.1 nm [10]. In 2017, H. Ahmad *et al.* proposed an multimode fiber interferometer combined with a Sagnac ring thulium-doped fiber laser, which achieved stable output from a single wavelength to up to 9 wavelengths [11]. In order to achieve stable multi-wavelength laser output, various specific fibers with different properties are often used to construct comb filters. Photonic crystal fiber begins playing an important role in the field of multi-wavelength fiber lasers because of its excellent performance.

Photonic crystal fiber (PCF) is a kind of waveguide based on photonic crystal and fiber manufacturing technology [12]–[14]. In 1996, the University of Southampton successfully pulled the world's first PCF by the bundle stacking method [15]. The hollow pores in the optical fiber are arranged in a periodic hexagonal pattern, and the core is formed by removing the air holes in the center of the optical fiber. The optical fiber maintains single-mode transmission with small loss. These properties encouraged the rapid development and extensive study of PCF. In 2015, Hameed. M. F *et al.* proposed a tunable polarization filter that fills the air holes of a PCF with liquid crystals [16]. The polarization filter is tuned by applying a voltage to change the properties of the liquid crystals. In 2018, Tian Y *et al.* proposed a PCF with rectangular air holes in the core, which can support transmission in the terahertz band with small dispersion [17]. As photonic information technology continues to develop, hollow PCF and multi-core PCF with different structures appear in different application fields, and PCF has become a research hotspot in the field of optics [18]–[21]. Because of its special optical guiding mechanism, PCF has advantages over ordinary single-mode fiber, such as infinite single mode, dispersion adjustable, large mode field, high nonlinearity, and high birefringence [22]–[25].

In this letter, we propose a TDFL with a ring cavity structure, which uses high birefringent PCF to make a Sagnac loop mirror while relying on the NPR effect to suppress mode competition of the output wavelengths. High birefringence PCF has extremely high birefringence coefficient, low bend-induced coupling between polarization states, our filter has advantages in extinction ratio and stability compared with non-PCF Sagnac loop. Theoretical simulation shows the free spectral range (FSR) of Sagnac loop mirror is 4.56 nm. By tuning the polarization controllers, the proposed all-fiber scheme allows stable multi-wavelength lasing oscillation with PCF-Sagnac at the near 2 μm spectral region.

Manuscript received September 8, 2021; revised January 6, 2022; accepted January 27, 2022. Date of publication February 1, 2022; date of current version February 11, 2022. This work was supported by the National Natural Science Foundation of China under Grants 61620106014 and 61827818. *(Corresponding author: Fengping Yan.)*

Ting Li, Fengping Yan, Wenguo Han, Ying Guo, Qi Qin, Zhuoya Bai, Dan Cheng, and Dandan Yang are with the School of Electronic and Information Engineering, Beijing Jiaotong University, Beijing 100044, China (e-mail: 19111024@bjtu.edu.cn; fpyan@bjtu.edu.cn; 14111021@bjtu.edu.cn; 18111014@bjtu.edu.cn; 19111034@bjtu.edu.cn; 16111003@bjtu.edu.cn; 16111004@bjtu.edu.cn; 21111013@bjtu.edu.cn).

Ting Feng is with the Photonics Information Innovation Center, Hebei Provincial Center for Optical Sensing Innovations, College of Physics Science and Technology, Hebei University, Baoding 071002, China (e-mail: wlxyft@hbu.edu.cn).

Digital Object Identifier 10.1109/JPHOT.2022.3147793

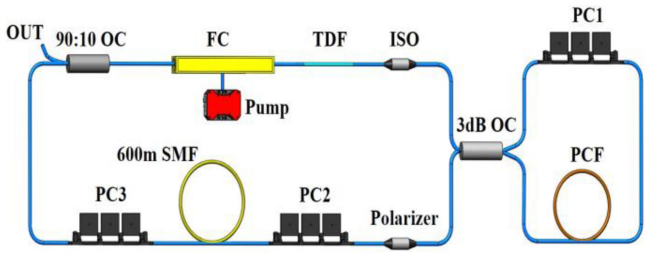

Fig. 1. The experimental step of the proposed multi-wavelength fiber laser.

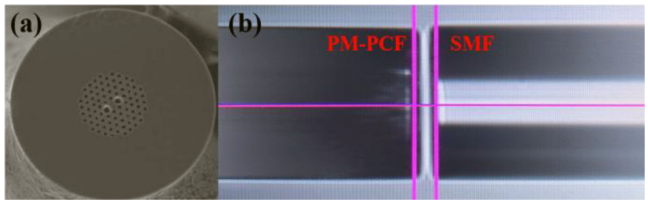

Fig. 2. (a) The sectional view of PCF. (b) The fusion splitter connects the PCF and SMF.

II. Experimental Step and Principle

The experimental setup of the proposed multi-wavelength TDFL is shown in Fig. 1.

A 793 nm laser diode (LD) with a 15 W maximum output power is used as the pump source. A 793/2000 nm fiber combiner (FC) connects the laser cavity to the pump source. The gain medium is a 2.5 m commercial double-clad Tm^{3+}-doped silica fiber (TDF) with a core diameter of 6.3 μm and inter-cladding diameter of 125 μm. Its adsorption at 793 nm is 1.4 dBm^{-1}. A PCF-Sagnac is used as the filter module, which consists of a 3 dB coupler, a polarization controller (PC), and 0.5 m PCF. The birefringence coefficient of PCF is 17.56×10^{-4}. A polarizer, two PCs and a 600 m SMF construct an NPR unit to inhibit the gain competition. The 600 m SMF provides the nonlinear phase shift, while the polarizer provides the NPR effect with adjustment of two PCs. The isolator (ISO) is used to ensure the clockwise operation. This TDFL outputs 10% power via the 90:10 coupler, and the laser output is monitored by an optical spectrum analyzer (YOKOGAWA AQ6375, OSA) with a resolution of 0.05 nm.

As shown in Fig. 2(a), the PCF has strong form birefringence and is optimized to create a short beat length between the polarization modes. It has reduced bend-induced coupling between polarization states, an improved polarization extinction ratio, and is 30 times less temperature-sensitive than conventional Hi-Bi fiber. Despite these desirable characteristics, several difficulties arise in practice. The air hole of the PCF will collapse due to welding electrode discharge when PCF is fused with SMF, which will lead to greater splicing loss. To protect the waveguide structure of PCF, we use the alignment function of fusion splicer to adjust PCF and SMF fiber cores on the same horizontal axis. Then, the two optical fiber ends are brought as close as possible by manual adjustment, as shown in Fig. 2(b), minimizing the splicing loss.

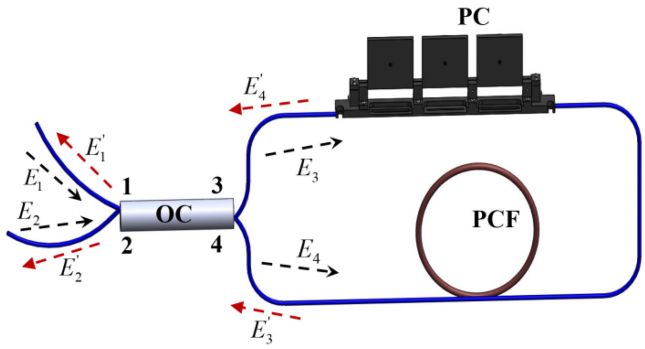

Fig. 3. The structure of PCF-Sagnac.

A. Transfer Characteristic of Sagnac Loop Mirror

As shown in Fig. 1, the Sagnac loop mirror is an all-fiber multi-wavelength comb filter that is simple to fabricate. The basic structure of the Sagnac ring is shown in Fig. 3. The device consists of a high-birefringent PCF, a 3 dB coupler, and a PC.

As shown in Fig. 3, when the signal light is input into the 3 dB coupler from port 1, it is divided into 50 percent clockwise transmission from port 3 and 50 percent counterclockwise transmission from port 4. When the light passes through the PCF, the phase difference between the fast axis and the slow axis will occur, and the direction of the polarized light will be rotated by an angle. When the light passes through the PC, the direction of the polarized light will be rotated by another angle. The last two beams of light in opposite directions were transmitted through PMF and PC for one week respectively, and coherent output was realized at the 3 dB coupler. The transmission characteristics of Sagnac loop mirror were analyzed using the Jones matrix:

$$E_{in} = \begin{bmatrix} E_x(t) \\ E_y(t) \end{bmatrix} \tag{1}$$

When the incident light passes through the 3 dB coupler, according to the theory of optical waveguide, the Jones matrix of the coupler is:

$$J_C = \begin{bmatrix} \sqrt{1-k} & j\sqrt{k} \\ j\sqrt{k} & \sqrt{1-k} \end{bmatrix} = \frac{\sqrt{2}}{2}\begin{bmatrix} 1 & j \\ j & 1 \end{bmatrix} \tag{2}$$

Where k represents the coupler spectral ratio, the Jones matrix of PCF and PC is:

$$J_{PMF} = \begin{bmatrix} e^{-j\varphi} & 0 \\ 0 & e^{j\varphi} \end{bmatrix}$$

$$\varphi = \pi \Delta n L/\lambda$$

$$J_{PC} = \begin{bmatrix} \cos\theta & \sin\theta \\ -\sin\theta & \cos\theta \end{bmatrix} \tag{3}$$

where Δn is the effective refractive index difference between fast and slow axis of PCF, L is the length of PCF, θ is the rotation angle of light wave in the direction of polarization. As a result, the E_3 and E_4 can be expressed as:

$$\begin{bmatrix} E_3 \\ E_4 \end{bmatrix} = \frac{\sqrt{2}}{2}\begin{bmatrix} 1 & j \\ j & 1 \end{bmatrix} \bullet \begin{bmatrix} E_1 \\ E_2 \end{bmatrix} \tag{4}$$

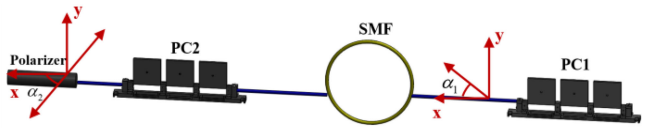

Fig. 4. The structure of NPR unit.

E_3' is the light field vector after E_3 passes PC and PCF, E_4' is the officialdom vector after E_4 passes PCF and PC:

$$E_3' = \begin{bmatrix} e^{-j\varphi} & 0 \\ 0 & e^{j\varphi} \end{bmatrix} \begin{bmatrix} \cos\theta_1 & \sin\theta_1 \\ -\sin\theta_1 & \cos\theta_1 \end{bmatrix} E_3$$

$$E_4' = \begin{bmatrix} \cos\theta_1 & -\sin\theta_1 \\ \sin\theta_1 & \cos\theta_1 \end{bmatrix} \begin{bmatrix} e^{-j\varphi} & 0 \\ 0 & e^{j\varphi} \end{bmatrix} E_4 \tag{5}$$

After E_3' and E_4' reach the coupler and coherent stacking, they are reflected from the coupler port 1 and transmitted from the coupler port 2:

$$\begin{bmatrix} E_1' \\ E_2' \end{bmatrix} = \frac{\sqrt{2}}{2} \begin{bmatrix} 1 & j \\ j & 1 \end{bmatrix} \bullet \begin{bmatrix} E_4' \\ E_3' \end{bmatrix} \tag{6}$$

From above formula, the transmission ratio of Sagnac can be obtained as:

$$T = \sin^2\theta_1 \cos^2\varphi \tag{7}$$

The wavelength spacing in terms of free spectral range (FSR) is determined by the following equation:

$$\Delta\lambda = \frac{\lambda^2}{\Delta n L} \tag{8}$$

B. Transfer Characteristic of NPR

In order to obtain more stable multi-wavelength fiber laser output at room temperature, researchers have done a lot of research on how to suppress the power fluctuation between wavelengths caused by the gain competition. Polarization Hole Burning (PHB), Intensity-dependent loss (IDL), Four Wave Mixing (FWM), and so on. The principle of IDL is inserting an optical device in laser cavity, the higher power wavelength will suffer greater loss than lower power wavelength and the total gain of each wavelength can be adjusted automatically. Therefore, the gain competition can be suppressed and the stable multi-wavelengths output can be achieved. The main implementation methods of IDL are nonlinear polarization rotation (NPR) and nonlinear optical loop mirror (NOLM).

The gain competition suppression mechanism uses an NPR unit composed of two PCs, a Polarizer and SMF, as shown in Fig. 4. α_1 is the angle between the input signal's polarization direction and the SMF fast axis, and α_2 is the angle between the SMF fast axis and the polarization direction. Adjusting PC1 and PC2 can change α_1 and α_2. In the laser cavity, the linearly polarized light leaving the polarizer becomes elliptically polarized through PC2. According to the Kerr effect, the transmission of the light in the SMF will result in the rotation of the polarization state of the light, and the rotation angle is proportional to the intensity of the light. After PC1 adjustment, so that the specific polarization of light through NPR, the rest of the polarization of light is filter red out.

Assuming that the linearly polarized signal is represented as $E(t)$, then the light components in the x direction of the fast axis and y direction of the slow axis can be represented as:

$$\begin{cases} E_x(t) = E(t)\cos\alpha_1 \\ E_y(t) = E(t)\sin\alpha_1 \end{cases} \tag{9}$$

After transmitting through SMF:

$$\begin{cases} E_x'(t) = E(t)\cos\alpha_1 \exp(-j\phi_x) \\ E_y'(t) = E(t)\sin\alpha_1 \exp(-j\phi_x) \cdot \exp[-j(\Delta\phi_L + \Delta\phi_{NL})] \end{cases} \tag{10}$$

$$\begin{aligned} \phi_x &= (n_x + n_x^{NL})\beta L \\ \Delta\phi_L &= (n_y - n_x)\beta L = 2\pi(n_y - n_x)L/\lambda \\ \Delta\phi_{NL} &= n_2(\sin^2\alpha_1 - \cos^2\alpha_1)|E(t)|^2\beta L/3 \\ &= -2\pi n_2 P L \cos 2\alpha_1/\lambda A_{eff} \end{aligned} \tag{11}$$

Where, γ is the nonlinear coefficient of the optical fiber, β is the transmission constant, L is the length of SMF between PC1 and PC2, P is the instantaneous power of the input signal, n_x and n_y are the linear birefringent coefficient respectively, n_x^{NL} and n_y^{NL} are the nonlinear birefringent coefficient, which are determined by the strength of the input signal and can be expressed as:

$$\begin{cases} n_x^{NL} = n_2\left(|E_x|^2 + \frac{2}{3}|E_y|^2\right) \\ = n_2|E(t)|^2\left(\cos^2\alpha_1 + \frac{2}{3}\sin^2\alpha_1\right) \\ n_y^{NL} = n_2\left(|E_y|^2 + \frac{2}{3}|E_x|^2\right) \\ = n_2|E(t)|^2\left(\sin^2\alpha_1 + \frac{2}{3}\cos^2\alpha_1\right) \end{cases} \tag{12}$$

When the signal light passed into the polarizer, the orthogonal components $E_x'(t)$ and $E_y'(t)$ interfere, and the output signal is:

$$\begin{aligned} E''(t) &= E'_x(t)\cos\alpha_2 + E'_y(t)\sin\alpha_2 \\ &= E'_x(t)\exp(-\mathrm{j}\phi_x)\{\cos\alpha_1\cos\alpha_2 \\ &\quad + \sin\alpha_1\sin\alpha_2\exp[-\mathrm{j}(\Delta\phi_L + \Delta\phi_{NL})]\} \end{aligned} \tag{13}$$

The transmission rate T_{NPR} introduced by NPR can be expressed as:

$$\begin{aligned} T_{NPR} &= |E''|^2 \big/ |E|^2 \\ &= \cos^2\alpha_1\cos^2\alpha_2 + \sin^2\alpha_1\sin^2\alpha_2 \\ &\quad + \frac{1}{2}\sin 2\alpha_1 \sin 2\alpha_2 \cos(\Delta\phi_L + \Delta\phi_{NL}) \end{aligned} \tag{14}$$

According to the above analysis, the transmission rate of NPR is related to the instantaneous power of input signal and the angle of two PCs. When α_1 and α_2 are different values randomly, the influence of P on NPR transmission is shown in Fig. 5. When α_1 and α_2 are fixed, the incident light with different instantaneous power has different transmittance when passing through the NPR unit. Therefore, different equalization effects can be obtained by adjusting α_1 and α_2.

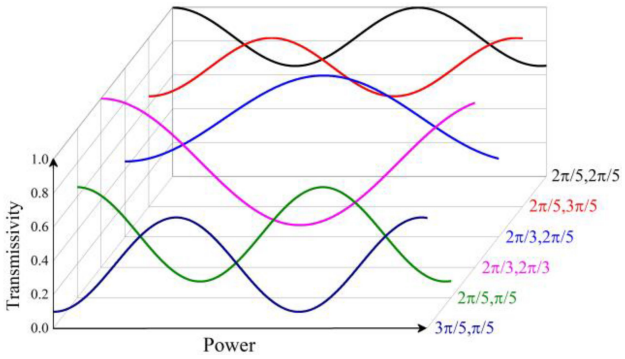

Fig. 5. The transmissivity of the NPR unit versus P under different α_1 and α_2 when used 600 m SMF.

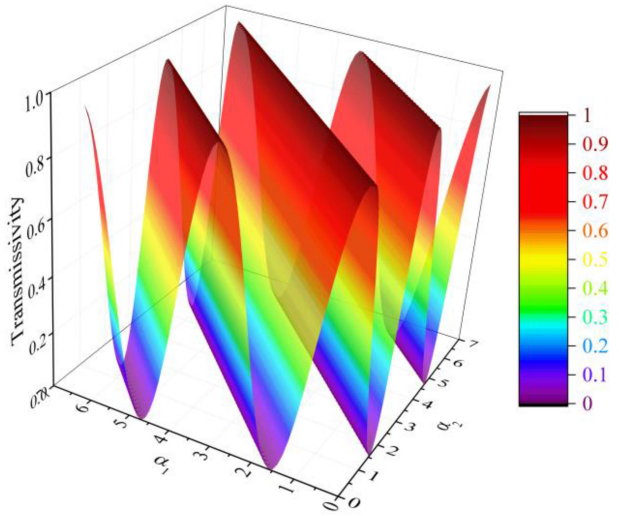

Fig. 6. Transmissivity of the NPR unit versus α_1 and α_2 with a fixed *P*.

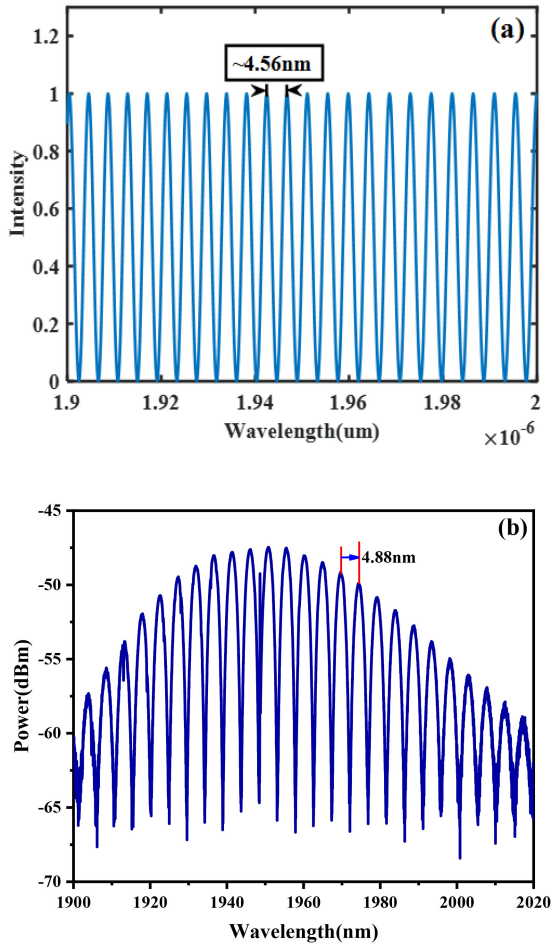

Fig. 7. Transmission spectra of the PCF-Sagnac filter. (a) Simulation. (b) Experiment.

When the length of SMF and instantaneous power *P* of the input signal are constant, different equalization effects can be obtained by adjusting α_1 and α_2, which can suppress the gain competition and achieve multi-wavelength output, as shown in Fig. 6.

Based on the equation, the FSR of the PCF-Sagnac is inversely proportional to the birefringence and the length of the PCF. The PCF-Sagnac transmission matrix was simulated and calculated, selecting θ as $\pi/2$, a wavelength range of 1900 to 2000 nm, and a PCF length of 0.5 m. The results of this simulation are shown in Fig. 7(a).

Fig. 7(b) shows the transmission spectrum of the PCF-Sagnac. A super continuous laser was used as the white-light source to prove the comb filter transmission function of PCF-Sagnac loop. The length of 0.5 m PCF corresponded to an adjacent wavelength spacing of 4.88 nm. The simulation results agree with the measurement results. The relative transmission spectrum of the PCF-Sagnac filter was obtained by subtracting the transmission spectrum of the PCF-Sagnac filter from the amplified spontaneous emission (ASE) spectrum.

III. Results and Discussion

With the experimental system described above, we modulated the number of stable output wavelengths from single to multi-wavelength by controlling the pump power and adjusting PCs. When the power of the 793 nm pump was fixed at 3.25 W, the gain and loss in the laser cavity reach equilibrium and a stable single wavelength operation was obtained.

As shown in Fig. 8, the central wavelength of the output laser is 1961.12 nm, with an OSNR of ~44 dB. To test output stability, the central wavelength was operated over 60 min without any adjustment to the fiber laser during the measurement.

The obtained output spectra are shown in Fig. 9(a), and the fluctuations of the central wavelength and output power are shown in Fig. 9(b). The power variation was less than ±0.30 dB, and no obvious wavelength drift was observed at the resolution of 0.05 nm of the OSA over 60 min at room temperature. This indicates that our TDFL can operate stably in single-wavelength lasing.

As shown in Fig. 10, through adjusting the PCs, the laser can perform stable multi-wavelength output. When PC1 is fixed in an appropriate state and the pump power is 5.83 W, irregular lasing

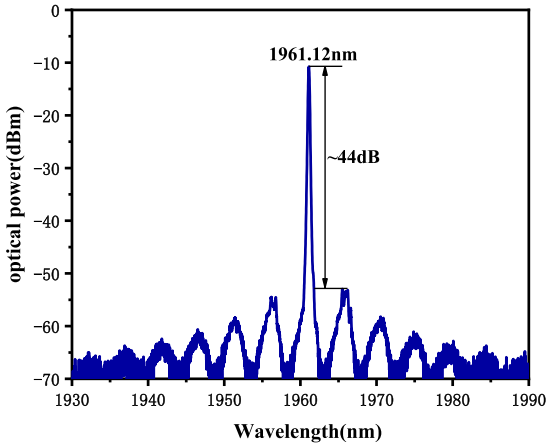

Fig. 8. Output spectra of single wavelength lasing.

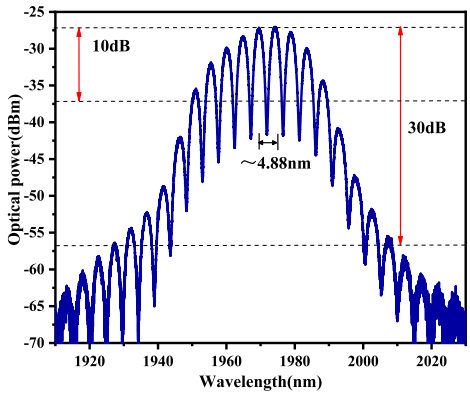

Fig. 10. Output spectra of multi-wavelength lasing.

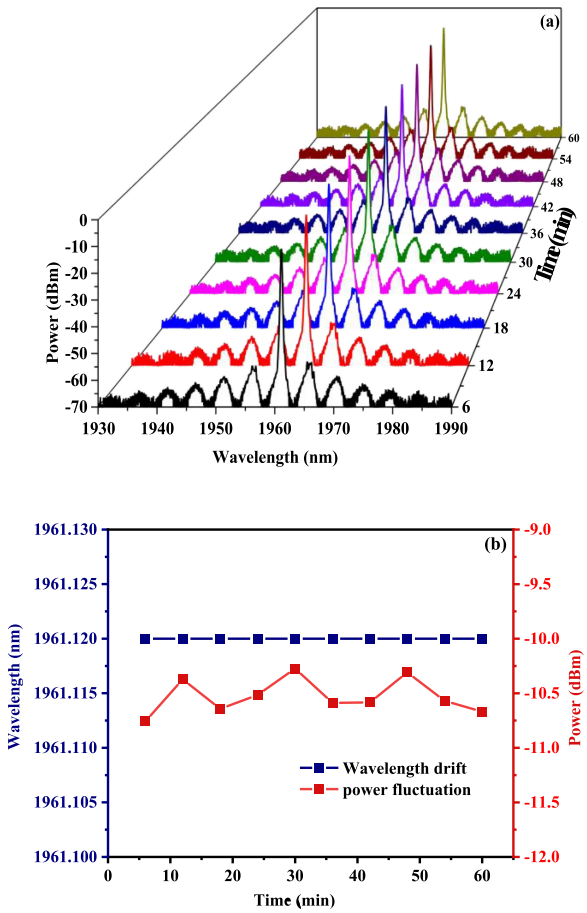

Fig. 9. (a) Measurement of the output spectra for ten times OSA scans with the time interval of six minutes, (b) fluctuations of the center wavelength and output power, respectively.

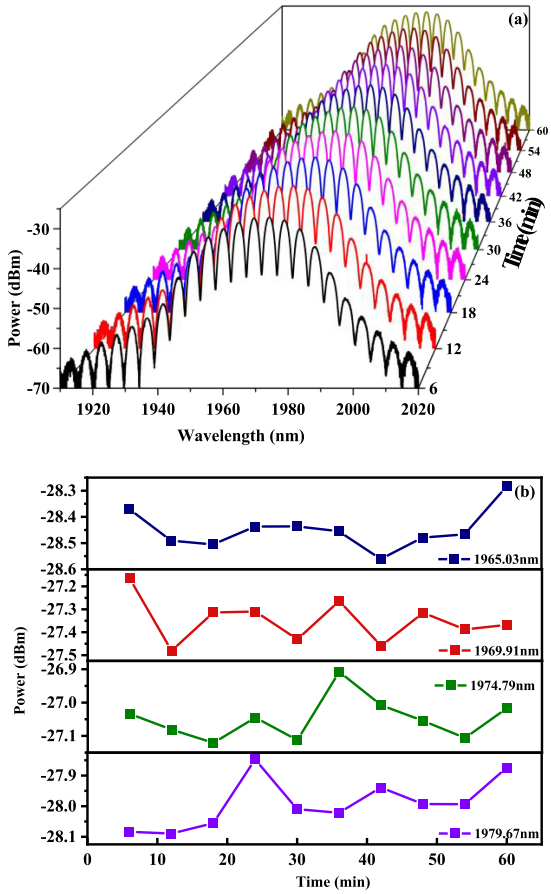

Fig. 11. (a) Measurement of the output spectra for ten times OSA scans with the time interval of six minutes, (b) fluctuations of the center wavelength and output power, respectively.

wavelength can be observed in OSA. By adjusting the polarization state of both PC1 and PC2, the NPR unit begins to inhibit mode competition, and stable multi-wavelength operation of the Tm^{3+}-doped silica fiber laser is obtained. It can achieve nine output channels within a 10 dB bandwidth from 1950.39 to 1989.43 nm. The channel spacing of the multi-wavelength TDFL is 4.88 nm, which is almost equal to the value of FSR calculated via simulation. The OSNR is better than 30 dB.

Fig. 11 shows the stability of the multi-wavelength TDFL. The optical spectrum was measured over 60 min with intervals of 6 min. The power variations of four individual channels: 1965.03, 1969.91, 1974.79, and 1979.67 nm, are presented in Fig. 11(b). The peak power variation of the laser is less than

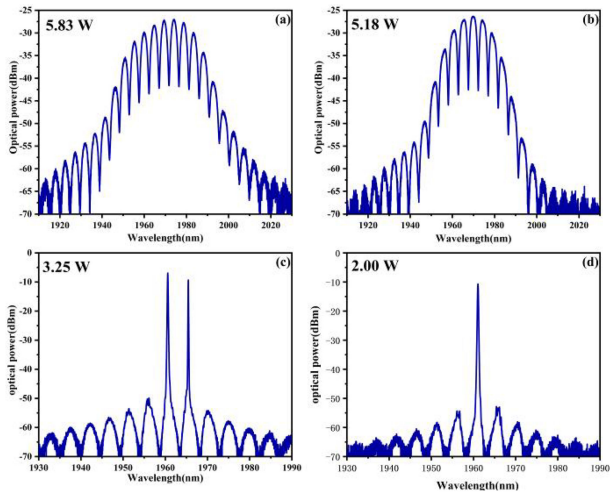

Fig. 12. Output spectrum of multiwavelength operation with different pump powers. (a) 5.83 W; (b) 5.18 W; (c) 3.25 W; (d) 2.00 W.

TABLE I
COMPARISON TABLE BETWEEN PUMP POWER AND MAXIMUM OSNR OF OUTPUT

Pump power	The number of wavelengths	The maximum OSNR
2 W	Single wavelength	44 dB
3.25 W	Dual wavelength	45 dB
5.18 W	Six wavelengths	33 dB
5.83 W	Nine wavelengths	30 dB

0.3 dB, indicating that the multi-wavelength TDFL can steadily operate at room temperature.

To study the influence of different pump powers on the multi-wavelength output characteristics of the fiber laser, the polarization state of the PCs was held constant. Fig. 12 shows the spectrum of multi-wavelength operation with pump power decreasing from 5.80 W to 2.00 W. More output channels are generated as the gain of the Tm^{3+}-doped silica fiber increases. Only one output channel with 40 dB OSNR is generated at the pump power of 2.00 W and 9 output channels within a 10 dB bandwidth are generated at the pump power of 5.80 W. Table I shows the relationship between pump power and the maximum OSNR of four output states:

With the increase of pumper power and output wavelengths, the maximum OSNR of four output states gradually decrease. This is caused by gain equalization of the NPR module, the output energy is dispersed and the power of each wavelengths are equalized.

IV. CONCLUSION

In this letter, we demonstrated a multi-wavelength Tm^{3+}-doped silica fiber laser based on a PCF-Sagnac loop. In the laser cavity, a Sagnac loop mirror containing 0.5 m PCF was used as the comb filter. When the FSR was ∼5 nm, the NPR fiber loop mirror of the laser cavity can overcome the mode competition. The number of channels increases as the power increases, and this configuration can achieve up to nine stable output channels by adjusting the PCs and pump power. These output channels are spaced at approximately 5 nm within a 10 dB bandwidth from 1951.11 to 1983.59 nm. Regardless of the operation wavelength, the OSNR of the TDFL was larger than 30 dB. Furthermore, if we splice PCF and SMF through employing befitting discharge parameter of fusion machine, the laser for lower insertion loss may be obtained, this is a very important point and will be left for future consideration. This research reveals that the proposed multi-wavelength thulium-doped fiber laser has up to nine stable wavelength outputs and greater than 30 dB OSNR, it can be an attractive candidate for dense wavelength division multiplexing systems in the era of rapid development of digital communication technology and comprehensive expansion of internet business.

REFERENCES

[1] H. Cheng *et al.*, "Numerical insights into the pulse instability in a GHz repetition-rate thulium-doped fiber laser," *J. Lightw. Technol.*, vol. 39, no. 5, pp. 1464–1470, 2021.
[2] Y. Xu *et al.*, "Dissipative soliton resonance in a wavelength-tunable thulium-doped fiber laser with net-normal dispersion," *IEEE Photon. J.*, vol. 7, no. 3, Jun. 2015, Art. no. 1502007.
[3] A. Sincore, J. D. Bradford, J. Cook, L. Shah, and M. C. Richardson, "High average power thulium-doped silica fiber lasers: Review of systems and concepts," *IEEE J. Sel. Topics Quantum Electron.*, vol. 24, no. 3, May/Jun. 2018, Art. no. 0901808.
[4] Z. Yan *et al.*, "Switchable multi-wavelength TM-doped mode-locked fiber laser," *Opt. Lett.*, vol. 40, no. 9, pp. 1916–1919, 2015.
[5] X. Wang, P. Zhou, X. Wang, H. Xiao, and L. Si, "Multiwavelength brillouin-thulium fiber laser," *IEEE Photon. J.*, vol. 6, no. 1, Feb. 2014, Art. no. 1500507.
[6] F. Yan, W. Peng, S. Liu, T. Feng, Z. Dong, and G. -K. Chang, "Dual-Wavelength single-longitudinal-mode tm-doped fiber laser using PM-CMFBG," *IEEE Photon. Technol. Lett.*, vol. 27, no. 9, pp. 951–954, May 2015.
[7] Z. Liu *et al.*, "High-capacity directly modulated optical transmitter for 2-μm spectral region," *J. Lightw. Technol.*, vol. 33, no. 7, pp. 1373–1379, Apr. 2015.
[8] W. Han *et al.*, "Wavelength-switchable single-longitudinal-mode thulium-doped fiber laser with sampled fiber Bragg grating," *IEEE Access*, vol. 9, pp. 62212–62218, 2021.
[9] J. X. B. Sia *et al.*, "1 × N (N = 2, 8) silicon selector switch for prospective technologies at the 2 μm waveband," *IEEE Photon. Technol. Lett.*, vol. 32, no. 18, pp. 1127–1130, Sep. 2020.
[10] H. Wei *et al.*, "A 1.8-μm multiwavelength thulium-doped fiber laser based on a hybrid interference filter," *Int. J. Optomechatronics*, vol. 10, no. 3/4, pp. 154–161, 2016.
[11] H. Ahmad *et al.*, "All-fiber multimode interferometer for the generation of a switchable multi-wavelength thulium-doped fiber laser," *Appl. Opt.*, vol. 56, no. 21, pp. 5865–5870, 2017.
[12] R. Soref, "The past, present, and future of silicon photonics," *IEEE J. Sel. Topics Quantum Electron.*, vol. 12, no. 6, pp. 1678–1687, Nov./Dec. 2006.
[13] J. N. Dash and R. Jha, "Graphene-based birefringent photonic crystal fiber sensor using surface plasmon resonance," *IEEE Photon. Technol. Lett.*, vol. 26, no. 11, pp. 1092–1095, Jun. 2014.
[14] K. Naeem *et al.*, "Simultaneous multi-parameter measurement using sagnac loop hybrid interferometer based on a highly birefringent photonic crystal fiber with two asymmetric cores," *Opt. Exp.*, vol. 23, no. 3, pp. 3589–3601, 2015.
[15] J. C. Knight, T. A. Birks, P. St. J. Russell, and D. M. Atkin, "All-silica single-mode optical fiber with photonic crystal cladding," *Opt. Lett.*, vol. 21, no. 19, pp. 1547–1549, 1996.
[16] M. F. Hameed *et al.*, "Ultra-high tunable liquid crystal-plasmonic photonic crystal fiber polarization filter," *Opt. Exp.*, vol. 23, no. 6, pp. 7007–7020, 2015.
[17] T. Yang *et al.*, "A scalable THz photonic crystal fiber with partially-slotted core that exhibits improved birefringence and reduced loss," *J. Lightw. Technol.*, vol. 36, no. 16, pp. 3408–3417, 2018.

[18] Z. Kakaie *et al.*, "Improvement of 2-μm thulium-doped fiber lasers via ASE suppression using all-solid low-pass photonic bandgap fibers," *J. Lightw. Technol.*, vol. 37, no. 22, pp. 5686–5691, 2019.

[19] K. Naeem, Y. Chung, and B. H. Kim, "Sagnac interferometer based on a highly-birefringent two-core PCF: Theory, experiment, and sensing characteristics," *J. Lightw. Technol.*, vol. 38, no. 18, pp. 5177–5190, 2020.

[20] Z. Tang *et al.*, "High performance tunable dual-wavelength erbium-doped fiber laser implemented by using tapered triple-core photonic crystal fiber," *IEEE Access*, vol. 8, pp. 121833–121842, 2020.

[21] H. Liu *et al.*, "Transverse-stress compensated methane sensor based on long-period grating in photonic crystal fiber," *IEEE Access*, vol. 7, pp. 175522–175530, 2019.

[22] N. Jahan *et al.*, "Photonic crystal fiber based biosensor for pseudomonas bacteria detection: A simulation study," *IEEE Access*, vol. 9, pp. 42206–42215, 2021.

[23] L. Velazquez-Ibarra *et al.*, "Tunable four-wave mixing light source based on photonic crystal fibers with variable chromatic dispersion," *J. Lightw. Technol.*, vol. 37, no. 22, pp. 5722–5726, 2019.

[24] M. Sharma *et al.*, "Giant nonlinear AlGaAs-doped glass photonic crystal fibers for efficient soliton generation at femtojoule energy," *IEEE Photon. J.*, vol. 11, no. 4, Aug. 2019, Art. no. 7102411.

[25] M. S. Hossain, S. M. A. Razzak, C. Markos, N. H. Hai, M. S. Habib, and M. S. Habib, "Highly birefringent, low-loss, and near-zero flat dispersion ENZ based THz photonic crystal fibers," *IEEE Photon. J.*, vol. 12, no. 3, Jun. 2020, Art. no. 7202109.